Structural Engineering and Mechanics, *Vol. 68, No. 2 (2018) 193-201*
DOI: https://doi.org/10.12989/sem.2018.68.2.193

Effects of loading history on seismic performance of SRC T-shaped column, Part I: Loading along web

J. Wang, Z.Q. Liu*, J.Y. Xue and C.M. Hu

College of Civil Engineering, Xi'an University of Architecture and Technology, Xi'an, China

(Received October 8, 2018, Revised July 14, 2018, Accepted August 20, 2018)

Abstract. This paper describes an experimental study on the seismic performance of steel reinforced concrete (SRC) T-shaped columns. The lateral loads were applied along the web of the column with different loading histories, such as monotonic loading, mixed loading of variable amplitude cyclic loading and monotonic loading, constant amplitude cyclic loading and variable amplitude cyclic loading. The failure modes, load-displacement curves, characteristic loads and displacements, ductility, strength and stiffness degradations and energy dissipation capacity of the column were analyzed. The effects of loading history on the seismic performance were focused on. The test results show that the specimens behaved differently in the aspects of the failure mode subject to different loading history, although all the failure modes can be summarized as flexural failure. The hysteretic loops of specimens are plump, and minimum values of the failure drift angles and ductility coefficients are 1/24 and 4.64, respectively, which reflect good seismic performance of SRC T-shaped column. With the increasing numbers of loading cycles, the column reveals lower bearing capacity and ductility. The strength and stiffness of the column with variable amplitude cyclic loading degrades more rapidly than that with constant amplitude cyclic loading, and the total cumulative dissipated energy of the former is less.

Keywords: steel reinforced concrete (SRC); T-shaped column; loading history; seismic performance; experimental study

1. Introduction

Steel reinforced concrete (SRC) special-shaped column structure is a new type of structural system developed in recent years. It enjoys the advantages of special-shaped column structure, such as making better use of available space and improving the esthetic appearance of structure (Wu and Xu 2009, Xiao *et al*. 2011a, Zhou *et al*. 2012a), and at the same time has the superiority of SRC structure, namely, high bearing capacity and good seismic performance (He *et al*. 2014a, Ellobody and Yong 2011b, Kim *et al*. 2012b). Therefore, SRC special-shaped column structure is favored by real estate developers and owners (Xue *et al*. 2014b).

T-shaped column, which is an important kind of special-shaped column, is usually used as exterior column (Fig. 1). Reinforced concrete (RC) T-shaped column has been extensively studied in the past few decades. Hsu (1989) examined twelve RC T-shaped column speciemens under biaxial bending and axial compression and a calculation method of ultimate bearing capacity was established. Mallikarjuna and Mahadevappa (1992) developed computer programs for RC T-shaped column to calculate the bearing capacity under biaxial eccentric compression. Balaji and Murty (2001) analyzed the reliability of RC T-shaped column sections by using the Monte Carlo simulation technique. In order to improve seismic performance, Cao *et al*. (2002) put forward RC T-shaped column with embedded column and tested four specimens under variable amplitude cyclic loading. However, very limited studies have been launched on SRC T-shaped column. Xue *et al*. (2012c, 2017) proposed the design formulas of ultimate shear strength and seismic damage calculation model for SRC T-shaped column. Chen *et al*. (2016) put forward the design limit values of axial compression ratio under different seismic grades for SRC T-shaped column. There is no other literature found to study on SRC T-shaped column. It is clear that the performance of SRC T-shaped column have not been fully addressed to date yet.

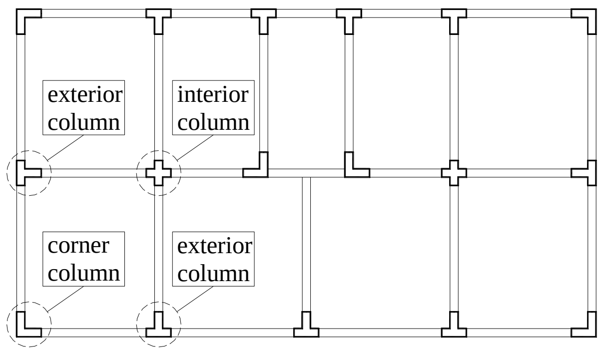

Fig. 1 Plan of special-shaped column structure

The seismic performance of a structure depends on its response, which in turn is a function of its loading history (Kumar and Usami 1996, Castiglioni 2005, Zheng *et al*.

*Corresponding author, Ph.D.
E-mail: liuzuqiang@xauat.edu.cn

Copyright © 2018 Techno-Press, Ltd.
http://www.techno-press.com/journals/sem&subpage=7
ISSN: 1225-4568 (Print), 1598-6217 (Online)

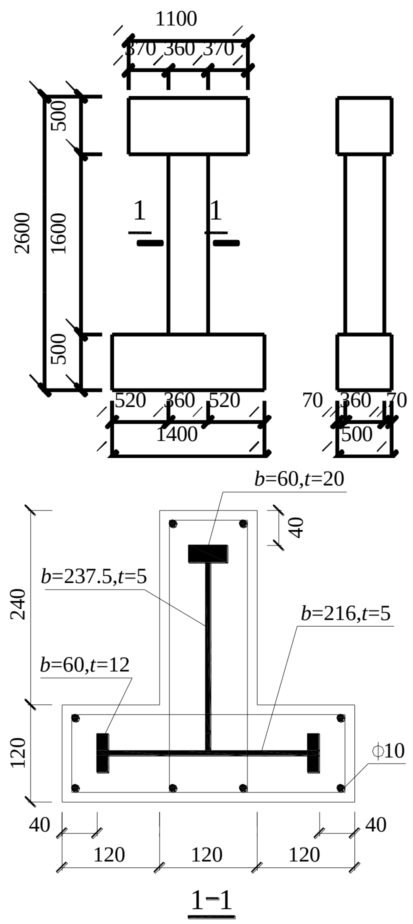

Fig. 2 Geometry and steel form of specimens

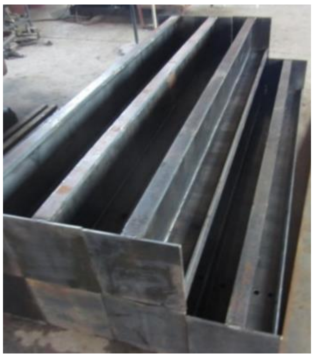

Fig. 3 Solid-web steel

Fig. 4 Steel skeleton

Table 1 Loading history of specimens

Specimen	T1	T2	T3	T4	T5	T6
Loading history	Monotonic loading	Mixed loading 1	Mixed loading 2	Mixed loading 3	Constant amplitude cyclic loading	Variable amplitude cyclic loading

Table 2 Mechanical properties of steel plates and longitudinal reinforcement

Material	Plate thickness (Diameter)	Yield strength f_y/MPa	Ultimate strength f_u/MPa	Elastic modulus E_s/MPa
Steel plate	5 mm	321.0	475.1	2.13×10^5
	12 mm	298.5	432.2	2.11×10^5
	20 mm	279.6	412.7	1.99×10^5
Longitudinal reinforcement	$\phi10$	369.0	518.7	2.10×10^5

2011c). In this paper, tests of six SRC T-shaped column specimens were carried out to investigate the seismic performance of the columns. The lateral loads were applied along the web of the column with different loading histories the failure mode, load-displacement curves, characteristic loads and displacements, ductility, strength and stiffness degradations and energy dissipation capacity of the columns are discussed in detail. Especially, the influences of the loading histories on the seismic performance are particularly looked into.

2. Experimental program

2.1 Specimen design

A total of six specimens of SRC T-shaped columns were constructed in the research program. In considerations of the available maximum loading capacity of the actuator and the conditions of the laboratory, the scale ratio of the specimens was determined as 1:2. All the column limb thicknesses were 120 mm with the sectional depth-thickness ratio of 3. Fig. 2 shows the geometry and steel form of SRC T-shaped column specimens. The shear-span ratio of 2.5 and the design axial compressive ratio of 0.4 were adopted for specimens. The changing parameter was loading history, including monotonic loading, mixed loading of variable amplitude cyclic loading and monotonic loading, constant amplitude cyclic loading and variable amplitude cyclic loading. The loading history of every specimen is listed in Table 1.

2.2 Fabrication and material properties

Specimens were configured with the solid-web steel, the steel ratio (namely, the cross-sectional area ratio between steel and column) of which was 7.09%. The Q235 steel plates were welded together to form solid-web steel (Fig. 3). The U-shaped or closed rectangular-shaped stirrups were welded on the solid-web steel, and the longitudinal reinforcements were assembled with the stirrups (Fig. 4). Φ 10 bars were used as longitudinal reinforcements, and Φ6 bars were used as stirrups, the interval of which was 60 mm. The reinforcement ratio was 0.873% and the stirrup ratio was 1.41%. The mechanical properties of steel plates and longitudinal reinforcement are given in Table 2.

Commercial concrete with aggregate diameter of 2.5-5 mm was used to pour specimens. The cubic concrete compressive strength measured at the 28th day was 34.5 MPa.

2.3 Test device and loading history

As shown in Fig. 5, the PCE device (PCE is the Japanese device for the pseudo-static experiment of structures) was used in this investigation, because it can simulate the force boundary conditions of actual structures (Fig. 6) more accurately than other devices (Chen *et al.* 2016). The axial compression load was applied to the specimen through a vertical jack and kept constant during the test process, and then lateral load was applied by horizontal actuator, which was controlled by MTS electro-hydraulic servosystem.

Lateral load was applied along the web (Fig. 7), and the loading history was divided into two phases. At the initial phase, the test was conducted under force control with the lateral load increasing 20 kN at every force level. When the specimen started yielding, the test was conducted under displacement control, and every displacement level increased Δ_y, which meant the yield displacement of the specimen. The test will be terminated after the lateral load decreased to about 85% of the maximum value. The specific loading histories are shown in Fig. 8.

(1) Monotonic loading: The force increased monotonically under force control, and then the displacement increased monotonically under displacement control. The loading history is shown in Fig. 8(a).

(2) Mixed loading: At first, one cycle at every force level was applied under force control. Then, three cycles at Δ_y for Mixed loading 1 (as shown in Fig. 8(b)), Δ_y and $2\Delta_y$ for Mixed loading 2 (as shown in Fig. 8(c)), and Δ_y, $2\Delta_y$ and $3\Delta_y$ for Mixed loading 3 (as shown in Fig. 8(d)) were applied under displacement control. Finally, the applied displacement increased monotonically under displacement control.

(3) Constant amplitude cyclic loading: The force increased monotonically under force control and the displacement increased to $2\Delta_y$ monotonically under displacement control. Then successive cycles at $2\Delta_y$ were applied under displacement control. The loading history is shown in Fig. 8(e).

(4) Variable amplitude cyclic loading: One cycle at every force level under force control, and then three cycles at every displacement level under displacement control. The loading history is shown in Fig. 8(f).

The horizontal displacement was measured by two linear variable differential transducers (LVDTs) at the top and mid-span of the column, and the lateral movement of the column basement was also measured, as shown in Fig. 7. The strains of solid-web steel and longitudinal reinforcements at the top and bottom of the column were measured by strain gages, and the measurement points are shown in Fig. 9, where S and B represent the measurement point of solid-web steel and longitudinal reinforcement, respectively. All data was collected by TDS-630 dynamic data acquisition instrument.

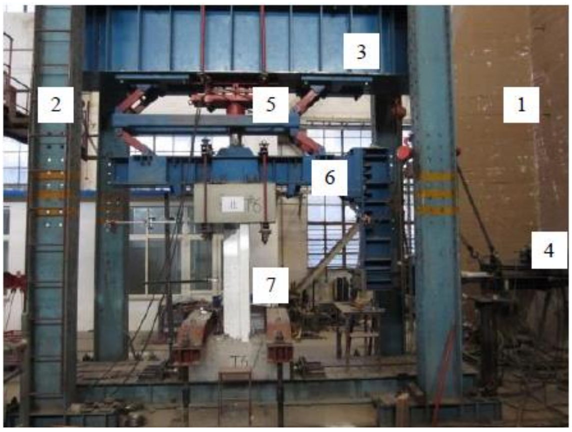

1 Reaction wall. 2 Reaction steel frame. 3 Reaction girder. 4 Horizontal actuator. 5 Vertical actuator. 6 PCE device. 7 Specimen

Fig. 5 Test setup

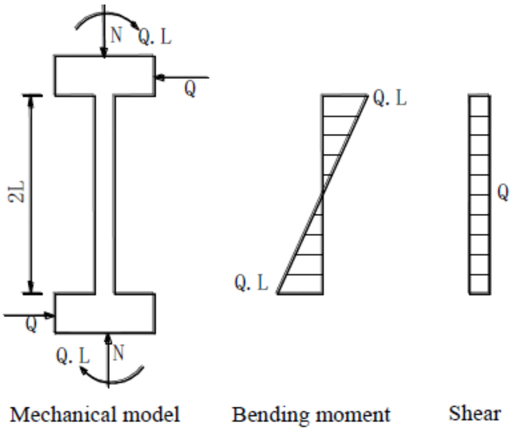

Fig. 6 Mechanical model for PCE device

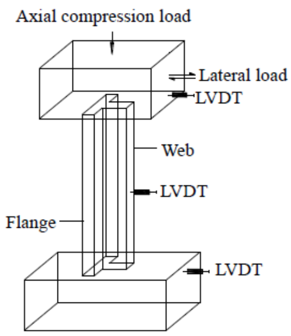

Fig. 7 Loading direction

3. Experimental results

3.1 Failure modes

Failure modes of specimens are shown in Fig. 10. All can be summarized as flexural failure. The failure process started from cracking of concrete, and then yielding of

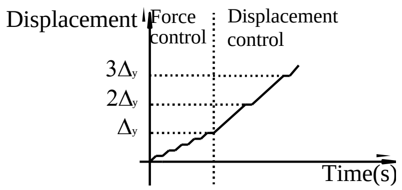

(a) Monotonic loading

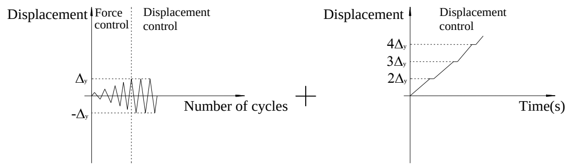

(b) Mixed loading1

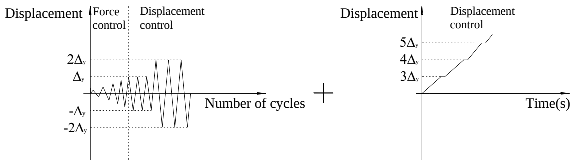

(c) Mixed loading 2

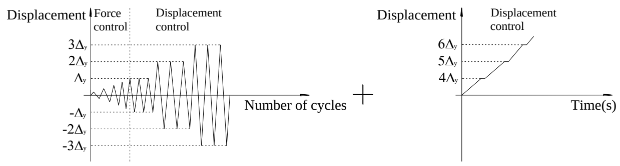

(d) Mixed loading 3

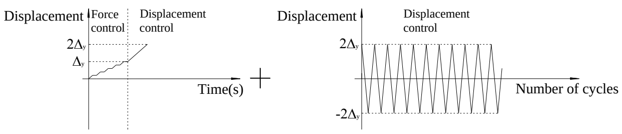

(e) Constant amplitude cyclic loading

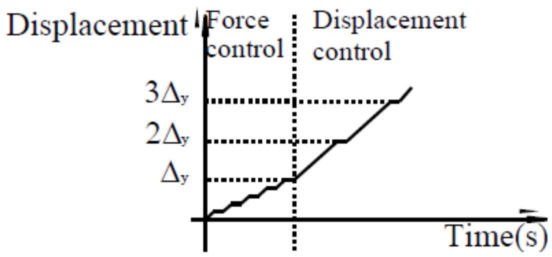

(f) Variable amplitude cyclic loading

Fig. 8 Loading history

longitudinal reinforcements and solid-web steel, crushing of concrete and buckling of longitudinal reinforcements appeared successively. The crushed concrete was the protective layer concrete, which was outside of solid-web steel and stirrups, while the concrete surrounded by the solid-web steel and stirrups basically remained intact. There was no local buckling occurred at the solid-web steel.

For specimen T1 which subjected to the monotonic loading, the web of top end and the flange of bottom end were in tension throughout the entire loading process. In these two regions, the transverse cracks appeared firstly, and became longer and wider as the applied force and displacement increased. Almost no concrete spalling was observed. For the compressive region located at the flange

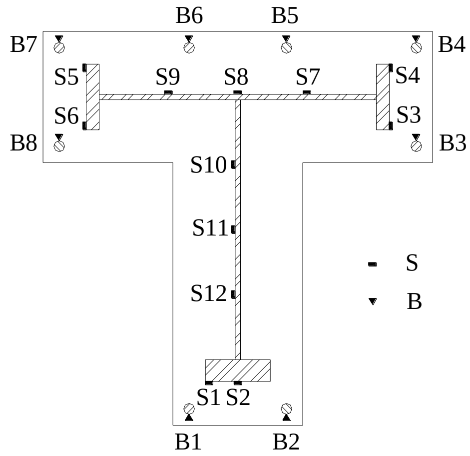

Fig. 9 Measurement points of strains

of top end and the web of bottom end, no evident crack was observed at the early stage until the concrete began to crush and dilated gradually with the increasing force and displacement.

For specimens T2, T3 and T4, low cyclic reversed loading was applied at the early stage of loading, resulting in that the tensile region and compressive region alternated between the web and flange of the column ends. Transverse cracks were observed at the surfaces of the column ends. Compressive damage of concrete also occurred, but the damaged degree of the three specimens with different loading histories was different. As the increasing numbers of loading cycles, the compressive damage of the specimen became more severe. For specimen T2, there was no crushing of concrete, and the crushing area of concrete of specimen T4 was larger than that of specimen T3. After cyclic loading, the monotonic loading was applied. Transvers cracks became wider and longer at the tensile regions and the crushing area of concrete expanded gradually at the compressive regions.

For specimens T5 and T6, low cyclic reversed loading was applied. Transverse cracks were observed at the web and flange of the column ends, and then concrete began to crush. For specimen T5, because of loading cycles with constant amplitude, the corresponding displacement of which was merely $2\Delta_y$, the crushing of concrete occurred only at the web of the column ends, and there was no crush of concrete at the flange. For specimen T6 with variable amplitude loading cycles, the damage was more serious and concrete crushed through the periphery of whole cross section of the column ends.

3.2 Load-displacement curves

Fig. 11 shows the load-displacement curves obtained in the tests, which illustrate the relationship between the lateral loads and displacements at the top end of column. In addition, except for specimen T5, the backbone curves at the positive direction of other specimens, which subjected to different numbers of loading cycle, are shown in Fig. 12. Based on Figs. 11 and 12, the following observations can be made:

(1) Before cracking, the loads and displacements had

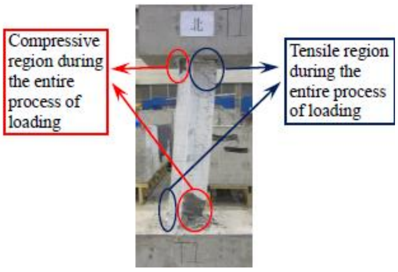

(a) T1

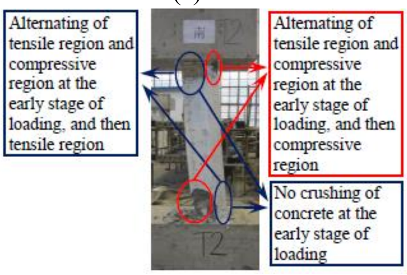

(b) T2

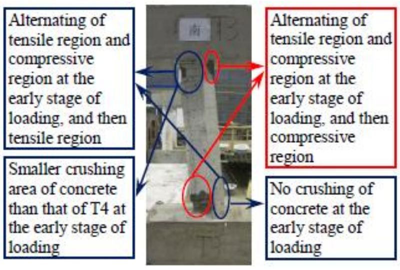

(c) T3

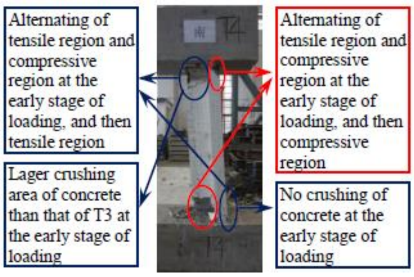

(d) T4

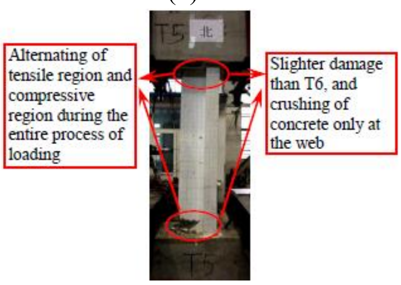

(e) T5

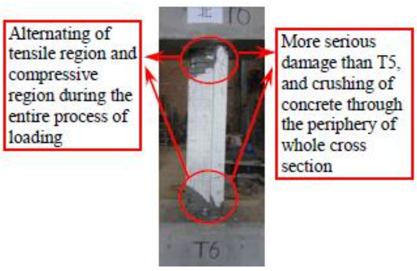

(f) T6

Fig. 10 Failure modes of specimens

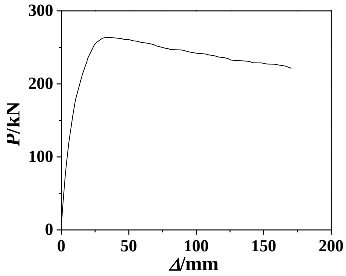

(a) T1

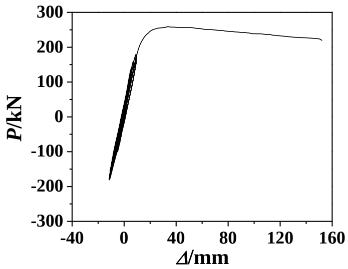

(b) T2

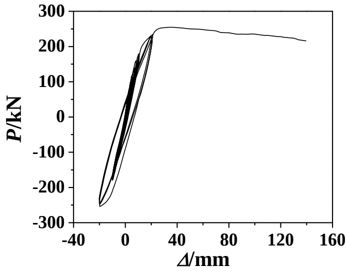

(c) T3

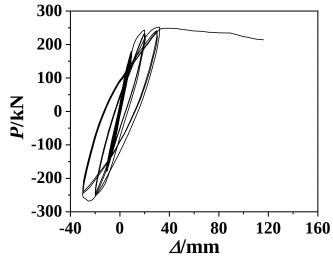

(d) T4

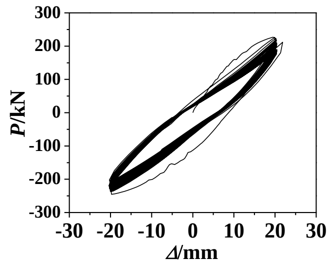

(e) T5

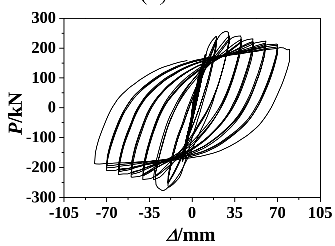

(f) T6

Fig. 11 Load-displacement curves

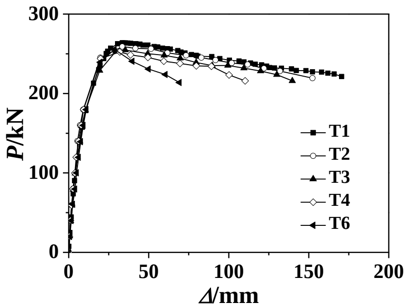

Fig. 12 Backbone curves

linear relationships, which indicated that specimens were in an elastic state. As cracks appeared at the column ends, the slope of load-displacement curves gradually decreases, and a larger residual deformation was observed when the lateral load was removed, indicating that specimens entered the elasto-plastic stage. After that, with the increasing of applied displacement, the load bore by specimens increased to the maximum and then began to decrease, and the stiffness degradation was obvious.

(2) Under cyclic loading, the spindle-shaped hysteretic loops of specimens indicate good energy dissipation capacity of SRC T-shaped column.

(3) The backbone curves of all five specimens overlapped at the elastic state, which demonstrated that the initial stiffness of the columns were similar, regardless of the loading histories. After that, the skeleton curves exhibited dramatic differences. The stiffness of specimens decreased rapidly with the increasing numbers of loading cycles.

3.3 Characteristic loads and displacements

In the sections of 3.3 and 3.4, the results of specimens T1, T2, T3, T4 and T6, of which the backbone curves are shown in Fig. 12, are compared.

Three critical characteristic points, namely, yield point, ultimate point and failure point can be obtained from the backbone curves as shown in Fig. 13, and the characteristic loads and displacements corresponding to these three points are listed in Table 3. The yield point (P_y, Δ_y) can be determined using the graphical method (Qian *et al*. 2014c), shown in Fig. 13. The ultimate load P_u is selected as the maximum load, and the failure load P_f is equal to $0.85P_u$.

Fig. 14 shows the effect of loading histories on the ultimate load. From Table 3 and Fig.14, it can be seen that compared with specimen T1, the ultimate load of specimens T2, T3 and T4 are 1.79%, 3.39% and 5.70% lower, respectively. This indicates that the bearing capacity of the column gradually decreases as the increasing numbers of loading cycles. However, the ultimate load of specimen T6 is higher than that of specimens T3 and T4, which is not conformed to the above law, and may result from the deviation of material strength.

In order to illustrate the ultimate deformation capacity better, the failure drift angles (θ_f) of specimens are listed in Table 3, which can be calculated as the ratio of failure displacement (Δ_f) to length of specimen. The effect of loading histories on the failure drift angles is shown in Fig.

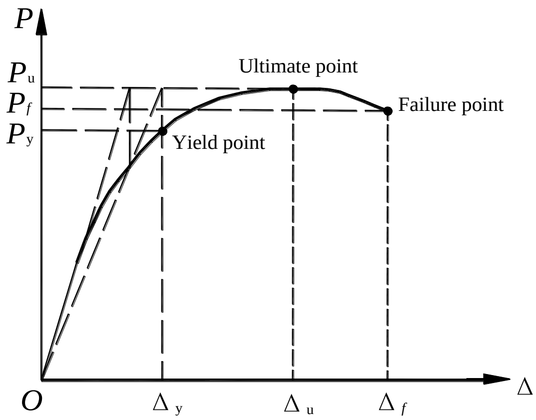

Fig. 13 Characteristic points on backbone curve

Table 3 Summary of measured results

Specimen	P_y / kN	D_y / mm	P_u / kN	D_u / mm	P_f / kN	D_f / mm	θ_f / rad	μ_Δ
T1	200.06	13.72	263.71	33.50	224.15	168.86	1/9	12.11
T2	198.88	12.81	258.99	33.49	220.14	151.82	1/11	11.85
T3	197.98	12.13	254.76	35.32	216.55	137.56	1/12	11.34
T4	196.15	12.01	248.68	38.65	211.38	121.19	1/13	10.09
T6	201.50	14.18	255.52	28.55	217.19	65.79	1/24	4.64

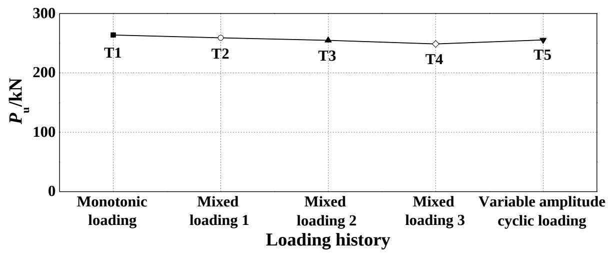

Fig. 14 The effect of loading histories on the ultimate load

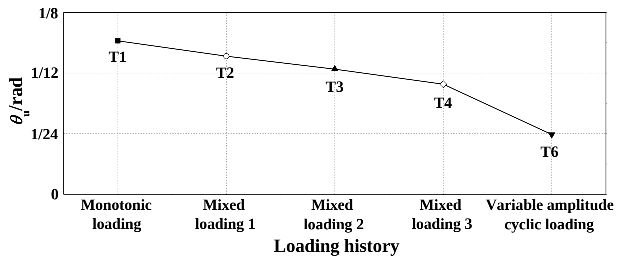

Fig. 15 The effect of loading histories on the failure drift angle

15. It can be seen that the failure drift angles of specimens are much larger than the limit value of reinforced concrete frame specified by Chinese seismic design code, which is equal to 1/50, indicating good collapse resistance capacity of SRC T-shaped column. As the increasing numbers of loading cycles, the ultimate deformation capacity of the column decreases significantly.

3.4 Ductility

Ductility is one of the most significant indexes to evaluate the seismic performance of a structure. The

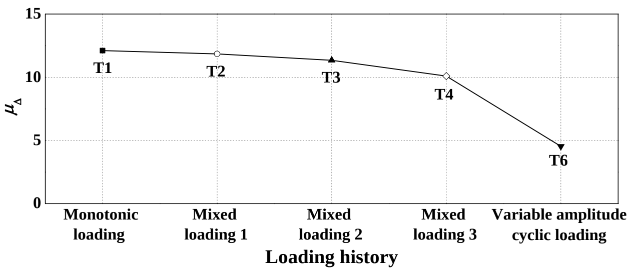

Fig. 16 The effect of loading histories on the displacement ductility coefficient

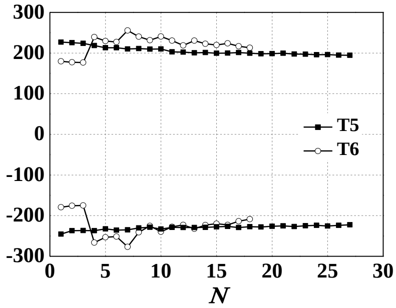

Fig. 17 Strength degradation

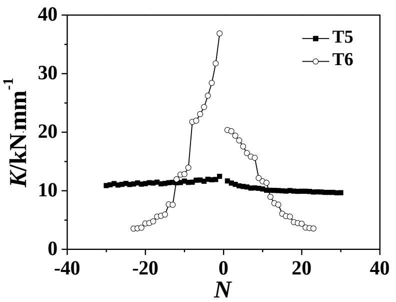

Fig. 18 Stiffness degradation

displacement ductility coefficient ($\mu_{\triangle}$) can be calculated as the ratio of failure displacement (Δ_f) to the yield displacement (Δ_y). The displacement ductility coefficients of specimens are listed in Table 3, all of which are larger than 4, indicating good ductility of SRC T-shaped column.

Fig. 16 illustrates the effect of loading histories on the displacement ductility coefficient. It can be seen that the ductility of the column deteriorates with the increasing numbers of loading cycles. Especially, the ductility of specimen T6, of which the displacement coefficient is less than 5, is much lower than that of other specimens, of which the displacement coefficients are larger than 10.

3.5 Strength degradation

In the sections of 3.5, 3.6 and 3.7, the results of specimen T5 subjected to constant amplitude cyclic loading are compared with that of specimen T6 subjected to variable amplitude cyclic loading.

It can be observed that the strength of the column specimen decreases at the same displacement level, which can be defined as strength degradation. Fig. 17 shows the strength (P) of both specimens versus number of cycles (N). For specimen T5, the strength degradation begins from the second cycle, of which the rate is slow during the entire process of loading. But the strength degradation of specimen T6 can be evidently observed due to the crushing of concrete, and until the displacement amplitude increases to $5\Delta_y$, the strength degradation tends to be slow, because the strength of the specimen was mainly provided by the solid-web steel at this time.

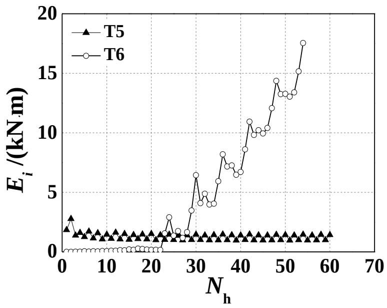

(a) Energy dissipated per semi-cycle versus number of semi-cycles

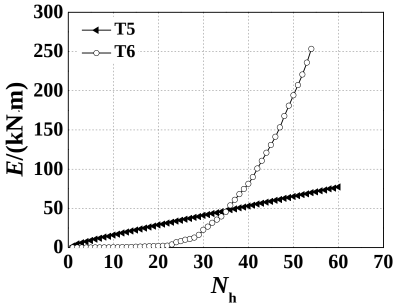

(b) Cumulative dissipated energy versus number of semi-cycles

Fig. 19 Energy dissipation capacity

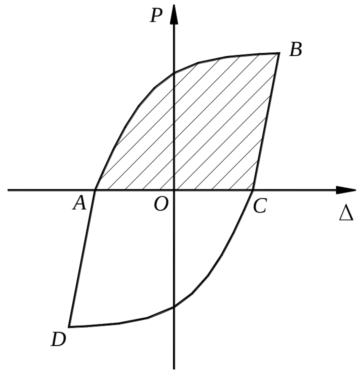

Fig. 20 Hysteretic loop

3.6 Stiffness degradation

The secant stiffness (Tao *et al.* 2013) of the column specimen decreases as the loading progresses, which can be defined as stiffness degradation. Fig. 18 shows the secant stiffness (K) of both specimens versus number of cycles (N). It can be seen that the initial stiffness of specimen T5 is much lower than that of specimen T6, but the rate of stiffness degradation of the former is much slower than that of the latter. There is no obvious abrupt change for the stiffness of specimen T5. On the contrary, the stiffness of specimen T6 degrades significantly, especially before the yielding of the specimen, when cracks appeared continuously.

3.7 Energy dissipation capacity

The energy dissipation capacity of a structure reflects the seismic energy absorption capability. Two indexes for evaluating the energy dissipation capacity are calculated from the load-displacement hysteretic loops and compared between the both specimens, as shown in Fig. 19, where E_i is the energy dissipated per semi-cycle, namely, the area of shadows in Fig. 20, N_h is the number of semi-cycles, and E is the cumulative dissipated energy. It can be seen that the energy dissipation capacity of specimen T5 under constant amplitude cyclic loading is almost unchanged with the increasing numbers of semi-cycles, while the energy dissipation capacity of specimen T6 under variable amplitude cyclic loading is evidently improved after yielding.

It must be noted that there are the results of specimen T5 subjected to 60 semi-cycles in Fig. 18, and the actual number of semi-cycles experienced by specimen T5 is 244 when it failed. Therefore, based on the approximate linear relationship between cumulative dissipated energy and number of semi-cycles, the total cumulative dissipated energy of specimen T5 can be calculated as about 300 kN·m, which is larger than that of specimen T6 as shown in Fig. 19(b).

4 Conclusions

This paper discusses the effects of loading history on the seismic performance of SRC T-shaped column. The conclusions are shown as the following:

(1) The failure modes of all the SRC T-shaped columns can be summarized as flexural failure, while the specimens behaved differently subject to different loading histories.

(2) The hysteretic loops of specimens are plump under cyclic loading, the failure drift angle is between 1/24 and 1/9, and the ductility coefficients are larger than 4. These indicate good seismic performance of SRC T-shaped column.

(3) With the increasing numbers of loading cycles, the bearing capacity and the ultimate deformation capacity of the columns decreases dramatically, and the ductility also decreases.

(4) Compared with constant amplitude cyclic loading, the strength and stiffness of the column under variable amplitude cyclic loading degrades more rapidly, and the total cumulative dissipated energy is less.

Acknowledgments

The authors would like to thank the Natural Science Foundation of China (Granted No. 51308444), Scientific Research Plan Project of Shaanxi Education Department (Granted No. 2018JM5124 and Program for Innovation Team of Xi'an University of Architecture and Technology for their supports of this study.

References

Balaji, K.V.G.D. and Murty, D.S.R. (2001), "Reliability analysis of RC T-shaped column sections", *Ind. Concrete J.*, **75**(3), 223-227.

Cao, W.L., Hu, G.Z., Cui, L.C., Zhou, M.J., Hao, C.S. and Qu, Y.H. (2002), "Experimental and analysis of seismic behavior of the +, L, T-shaped columns with concealed columns", *J. Build. Struct.*, **23**(1), 16-20.

Castiglioni, C.A. (2005), "Effects of the loading history on the local buckling behavior and failure mode of welded beam-to-column joints in moment-resisting steel frames", *J. Eng. Mech. ASCE*, **131**(6), 568-585.

Chen, Z.P., Xu, J.J., Chen, Y.L. and Xue, J.Y. (2016), "Axial compression ratio limit values for steel reinforced concrete (SRC) special-shaped columns", *Steel Compos. Struct.*, **20**(2), 295-316.

Ellobody, E. and Yong, B. (2011b), "Numerical simulation of concrete encased steel composite columns", *J. Constr. Steel Res.*, **67**(2), 211-222.

He, J., Liu, Y.Q., Chen, A.R., Wang, D.L. and Yoda, T. (2014a), "Bending behavior of concrete-encased composite I-girder with corrugated steel web", *Thin-Walled Struct.*, **74**, 70-84.

Hsu, T.C. (1989), "T-shaped reinforced concrete members under biaxial bending and axial compression", *ACI Struct. J.*, **86**(4), 460-468.

Kim, C.S., Park, H.G., Chung, K.S. (2012b), "Eccentric axial load testing for concrete-encased steel columns using 800 MPa steel and 100 MPa Concrete", *J. Struct. Eng.*, **138**(8), 1019-1031.

Kumar, S. and Usami, T. (1996), "Damage evaluation in steel box columns by cyclic loading tests", *J. Struct. Eng. ASCE*, **122**(6), 626-634.

Mallikarjuna and Mahadevappa P. (1994), "Computer aided analysis of reinforced concrete columns subjected to axial compression and bending-PartII: T-shaped Sections", *Comput. Struct.*, **53**(6), 1317-1356.

Qian, J.R., Li, N.B., Ji, X.D. and Zhao, Z.Z. (2014c), "Experimental study on the seismic behavior of high strength concrete filled double-tube columns", *Earthq. Eng. Eng. Vibr.*, **13**(1), 47-57.

Tao, M.X., Fan, J.S. and Nie, J.G. (2013), "Seismic behavior of steel reinforced concrete column-steel truss beam hybrid joints", *Eng. Struct.*, **56**, 1557-1569.

Wu, B. and Xu, Y.Y. (2009), "Behavior of axially-and-rotationally restrained concrete columns with '+'-shaped cross section and subjected to fire", *Fire Safe. J.*, **44**(2), 212-218.

Xiao, J.Z., Li, J. and Chen, J. (2011a), "Experimental study on the seismic response of braced reinforced concrete frame with irregular columns", *Earthq. Eng. Eng. Vibr.*, **10**(4), 487-494.

Xue, J.Y., Chen, Z.P., Zhao, H.T., Gao, L. and Liu, Z.Q. (2012c), "Shear mechanism and bearing capacity calculation on steel reinforced concrete special-shaped columns", *Steel Compos. Struct.*, **13**(5), 473-487.

Xue, J.Y., Gao, L., Liu, Z.Q., Zhao, H.T. and Chen, Z.P. (2014b), "Experimental study on mechanical performance of lattice steel reinforced concrete inner frame with irregular section columns", *Steel Compos. Struct.*, **16**(3), 253-267.

Xue, J.Y., Zhou, C.F. and Liu, Z.Q. (2017), "Research on damage of solid-web steel reinforced concrete T-shaped columns subjected to various loadings", *Steel Compos. Struct.*, **24**(4), 409-423.

Zheng, S.S., Wang, B., Li, L., Hou, P.J. and Wang, W. (2011c),

"Study on seismic damage of SRHSC frame columns", *Sci*. *China Tech*. *Sci*., **54**(11), 2886-2895.
Zhou, T., Chen, Z.H. and Liu, H.B. (2012a), "Seismic behavior of special shaped column composed of concrete filled steel tubes", *J. Constr*. *Steel Res*., **75**, 131-141.

PL